Exceptional surface states and topological order in Bi_2Se_3

Deepnarayan Biswas and Kalobaran Maiti*
Department of Condensed Matter Physics and Materials' Science,
Tata Institute of Fundamental Research, Homi Bhabha Road, Colaba, Mumbai - 400 005, India.
(Dated: June 13, 2015)

Topological insulators possess time reversal symmetry protected metallic surface states over the insulating bulk, where these surface states are expected to be immune to small disorder, chemical passivation of the surface or temperature change. However, significant discrepancy from such behavior has been found experimentally in various materials. Here, we review some of our recent results on the electronic structure of a typical topological insulator, Bi_2Se_3. Both, the band structure results and high resolution angle resolved photoemission data reveal significantly different surface electronic structure for different surface terminations. Furthermore, oxygen impurity on Se terminated surface exhibits an electron doping scenario, while oxygen on Bi terminated surface corresponds to a hole doping scenario. The intensity of the Dirac states reduces with aging indicating fragility of the topological order due to surface impurities.

PACS numbers: 73.20.At, 03.65.Vf, 68.43.-h

INTRODUCTION

Insulators are materials having an energy gap between the highest occupied band (valence band) and the lowest unoccupied band (conduction band). Topological insulators are a special type of such materials, which possess gapless states with novel electromagnetic properties protected by time reversal symmetry at the surface of bulk insulators [1, 2]. The speciality of these surface states is that they are protected from backscattering due to the time reversal symmetry as such processes in the presence of time reversal symmetry requires a spin-flip, which is different from a typical two-dimensional surface states. Thus, the electric current due to the topologically ordered states is expected to be non-dissipative. The topologically ordered energy bands exhibit linear dispersion forming a Dirac cone. The formation of such states requires strong spin-orbit coupling and breaking of inversion symmetry.

Topological insulators have been theoretically predicted [3] and presumably for the first time, experimentally observed in HgTe [4]. Since then enormous research has been carried out as these materials are expected to bring immense technological advances and new possibilities in the fields of spintronics, quantum computation, dissipationless charge transfer etc. [2]. Several materials have been discovered exhibiting surface states with topological order along with significant deviation from the theoretical predictions for such systems. For example, the bulk electronic structure of almost all the materials studied exhibits large density of states at the Fermi level [5]. Experiments show contrasting scenarios often with instability of the topologically ordered states. Thus, finding of an ideal topological insulator as per the definition continues to be an outstanding puzzle.

In this paper, we review some of our recent works on the stability of the topologically ordered surface states

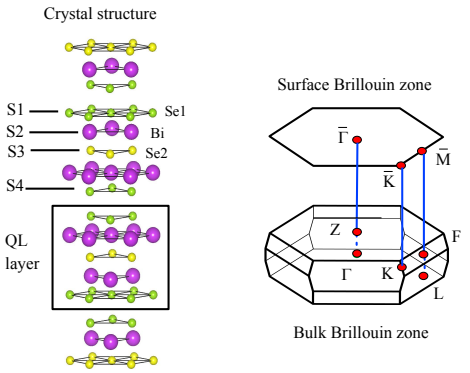

FIG. 1. Crystal structure of Bi_2Se_3 (left panel) and its Brillouin zone (right panel). Se1 and Se2 are two non-equivalent Se atoms. S1, S2, S3 and S4 are the surface layers for different surface terminations. The square box shows the quintuple layer.

of an archetypical topological insulator, Bi_2Se_3 [6, 7]. Bi_2Se_3 forms in a layered structure as shown in Fig. 1 with the quintuple layers of Se1-Bi-Se2-Bi-Se1 (Se1 and Se2 are the two non-equivalent Se atoms) stacked together by Van der Waals force [8]. The surface electronic structure of Bi_2Se_3 exhibits topological order with the apex of the Dirac cone, called the Dirac Point (DP) appearing far away from the Fermi level, E_F due to the charge carrier doping arising from impurities, imperfections, etc. [9–11]. These states often show instability with time and complex time evolutions [5, 12], which has been attributed to different phenomena such as relaxation of the Van der Waals bond [13], the surface band bending [5], dangling surface states [14], etc. Some ob-

Journal Ref: J. Elect. Spec. Relat. Phenom. 208, 90 (2016) http://dx.doi.org/10.1016/j.elspec.2015.11.007

servations indicate formation of two dimensional electron gas (2DEG) and Rashba states with time that has been explained employing impurity induced band bending scenario [15–17]. In order to reveal microscopic details underlying such complex electronic properties, we calculated the electronic band structure for both surface and bulk of the material employing density functional theory, and carried out high resolution photoemission measurements with angle resolution and varied bulk sensitivity. The experimental results show exceptional behavior of the surface states due to different terminations and aging, which could be corroborated well by band structure calculations.

EXPERIMENTAL AND THEORETICAL DETAILS

Photoemission measurements were carried out on single crystalline Bi_2Se_3 samples grown by Bridgemann method and characterized by x-ray diffraction, Laue diffraction etc. Hard x-ray photoemission (HXP) measurements were carried out using 5947.9 eV photon energy at the P09 beamline of Petra III, Hamburg, Germany and Phoibos analyzer (energy resolution = 150 meV). For angle resolved and conventional x-ray (Al $K\alpha$; $h\nu$ = 1486.6 eV) photoelectron spectroscopy (ARPES and XPS), a Gammadata Scienta R4000 WAL analyzer and monochromatic photon sources were used with energy resolution 10 meV and 380 meV, respectively and an angular resolution of about 0.1°. The pressure of the photoemission chamber was maintained at about 5×10^{-10} torr during the measurements with the photon sources on. The sample was cleaved in situ using a top post glued on top of the sample. The cleanliness of the cleaved sample surface was checked using XPS & HXP wide scans and the surface crystallinity was verified by sharp & intense low energy electron diffraction (LEED) spots. All the data presented here are collected at temperature below 30 K using an open cycle He cryostat.

The electronic band structure calculation of Bi_2Se_3 was carried out using full potential linearized augmented plane wave method [18]. The bulk electronic structure was calculated using the lattice constants, $a = b = 4.18$ Å, $c = 28.7$ Å, $\alpha = \beta = 90°$ and $\gamma = 120°$ obtained from Ref. [19]. In order to investigate the surface electronic structure, we considered the lattice in a 'slab' configuration with at least 5 quintuple layers within the unit cell - the total number of layers varies for different surface terminations. Calculations were carried out for the surface terminations, S1 (Se1 terminated), S2 (Bi terminated), S3 (Se2 terminated) and S4 (one Se1 layer over the quintuple layer) as defined in Fig. 1. We calculated the electronic structure for both the pristine surface and a layer of oxygen over it. The exchange and correlation potential was included using the generalized gradient approximation (GGA) [20] and the spin-orbit interaction was included for Bi and Se atoms. The energy convergence was achieved using $10 \times 10 \times 1$ k points mesh.

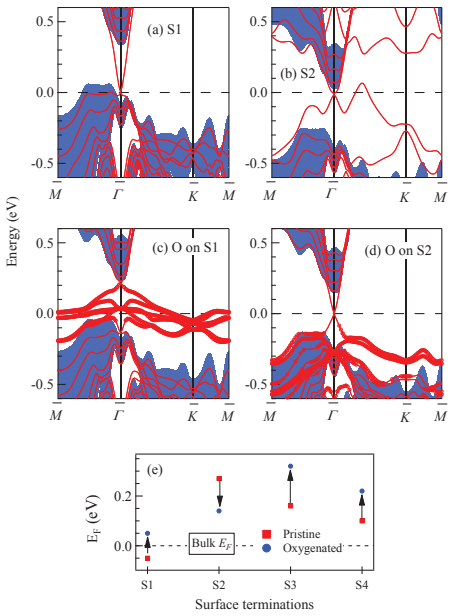

FIG. 2. Band structure results for (a) Se1 (S1-case) and (b) Bi (S2-case) terminated surface. The band structure for one layer oxygen deposited on S1 ans S2 terminations are shown in (c) and (d). (e) The Fermi level position with respect to the Bulk Fermi level.

RESULTS AND DISCUSSIONS

We studied the electronic band structure for four different surface terminations, S1, S2, S3 and S4 as shown in Fig. 1. The energy bands near ϵ_F consist primarily of Se $4p$ and Bi $6p$ characters. The results for all the surface terminations exhibit the surface bands crossing the Fermi level between surface projected time reversal invariant momenta (TRIM), $\bar{\Gamma}$-$\bar{M}$ odd number of times implying that the material belong to a strong topological insulator class [2, 7]. However, the signature of Dirac cone was observed only for Se1, Se2 and Bi terminated surfaces denoted by S1, S2 and S3, respectively. The S4 case (one Se1 layer over the quintuple layer) exhibits two dimensional surface states with no signature of the Dirac cone.

The calculated results [6] for experimentally observed surfaces, S1 and S2 terminations, are shown in Fig. 2. The lines show the results of the slab calculation and the shaded region represents the projected bulk bands (PBB). The inclusion of spin-orbit coupling in the calculation led to the Dirac cone like structure in the bands.

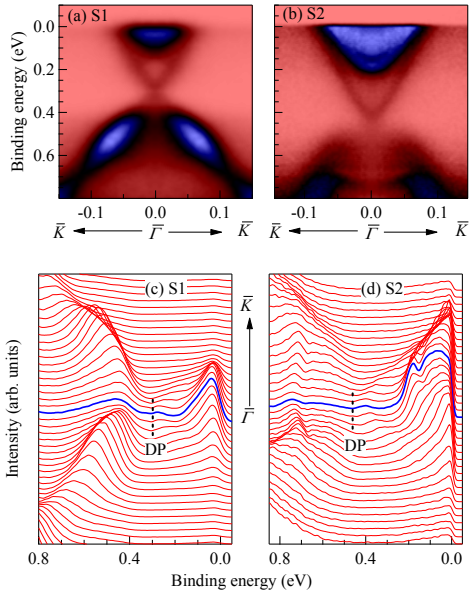

FIG. 3. ARPES spectra for (a) S1 and (b) S2 surface terminations. The corresponding energy distribution curves (EDC) are shown in (c) and (d).

The Dirac cone like structure in the energy band dispersion with DP at E_F is evident for both the surface terminations. DP appears close to the top of the valence band for Se terminated surface (S1 case) and in the vicinity of the bottom of the conduction band for Bi-terminated surface (S2 case).

Surface/bulk impurities and/or defects play an important role in the electronic structure leading to charge carrier doping, disorder induced local character to the charge carriers etc. [21–23] Since we observed signature of oxygen impurities on the sample surface with aging, we have calculated the electronic structure considering one monolayer (ML) oxygen on the surface. The presence of 1 ML oxygen on the S1 and S2 surfaces changes the bands near E_F drastically as shown in Figs. 2(c) and 2(d). The thick lines show the energy bands with at least 50% contribution from O $2p$. On Oxygen deposition, the DP on S1 shifts to higher binding energy and the O $2p$ contribution appears at the Fermi level. For S2 case, the DP becomes better defined and shifts away from the bulk conduction band due to oxygen deposition. Interestingly, O $2p$ states do not contribute to the Dirac cone. While O $2p$ bands appear at E_F with DP at higher binding energy in S1 case, the reverse scenario is observed in S2 case with DP at E_F and O $2p$ bands at higher binding energies. Thus, the Dirac states appear to be more accessible to derive various thermodynamic/electronic properties in the case of oxygen deposited Bi terminated surface.

Different surface termination of the samples results into significantly different chemical potential of the system as shown in Fig. 2(e), where E_F is shown with respect to the bulk E_F. While S2, S3 and S4 cases show an increase in Fermi energy, the Fermi energy becomes smaller than the bulk Fermi energy in S1 case. The Bi terminated surface exhibits the highest energy difference. Oxygen deposition leads to a shift of the Fermi level towards higher energies suggesting an effective electron doping into the system for all the Se terminations. The deposition of oxygen on Bi terminated surface (S2 case), on the other hand, leads to a shift of E_F in the opposite direction - towards lower energies suggesting an effective hole doping in this case.

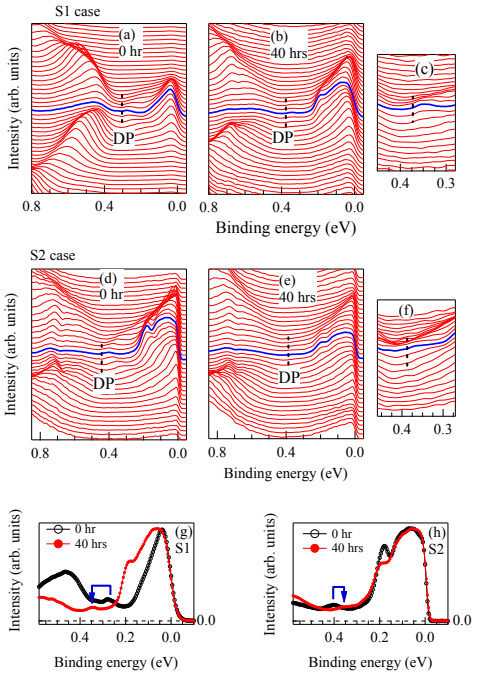

FIG. 4. EDCs collected at different time delays. S1-case: (a) 0 hr, (b) 40 hrs after cleaving [(c) rescaled 40 hrs delay data shown in (b)]. S2-case: (d) 0 hr, (e) 40 hrs [(f) rescaled 40 hrs data] after cleaving. Comparison of the 0 hr and 40 hrs delay spectra at Γ-point for (g) S1 and (h) S2 terminations.

Various experiments showed that exposure of different surface terminations is possible in samples having different concentration of defects/impurities in the sample. However, we observe exposure of different surface terminations on cleaving the same sample. The cleaving required a top post removal method indicating inter-quintuple layer coupling significantly strong. All these results indicate that the sample used in our study possessed a critical concentration of the defects that makes exposure of both surfaces possible, which enabled us to study the effect of different surface terminations without changing the defect/impurity level. The ARPES results on S1 and S2 terminations are shown in Fig. 3 - the characterization to S1 and S2 terminations is done later in the

text. In both the cases, the Dirac cone is manifested in the surface energy bands within the energy gap of the bulk bands. Interestingly, the DP appear at significantly different binding energies for these two cases; 0.3 eV and 0.45 eV for S1 and S2 terminations, respectively.

The most interesting phenomena occur with aging of the sample surfaces. The aging of S1 case is shown in Figs. 4(a), 4(b) [4(c) is the rescaled data shown in 4(b)] exhibiting a shift of DP towards higher binding energy indicating electron doping scenario. In contrast, Figs. 4(d), 4(e) [4(f) is the rescaled data shown in 4(e)] representing the S2 case exhibit a shift of the DP in the opposite direction - towards lower binding energy indicating a hole doping scenario. The shift of DP with aging has been observed in other studies, where the electronic structure changes could be attributed largely to the impurity/defect level present in the sample [12, 24]. However, the opposite shift of DP from the same sample for different surface termination is extraordinary and indicate the important role of surface terminations rather than the level of defects/impurities.

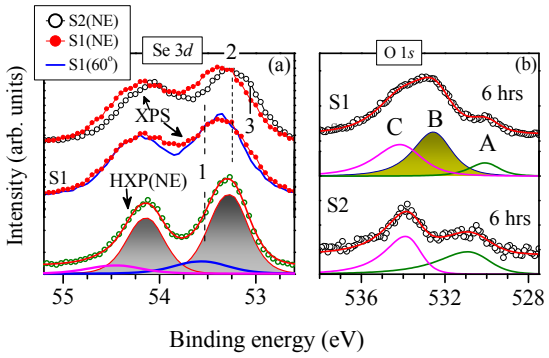

FIG. 5. (a) Top panel: Normal emission (NE) Se $3d$ core level spectra using Al $K\alpha$ source (XPS) for S1 (solid circle) and S2 (open circles) surfaces. Middle panel: Al $K\alpha$ spectra for S1 surface collected at normal emission (solid circles) and 60° angled emission (line). Lower panel: Hard x-ray spectrum (HXP) at normal emission from S1 surface. The lines represent the fit of the spectrum and component peaks. (b) O $1s$ spectra from S1 and S2 terminations after 6 hours of cleaving. Lines are the corresponding fit data.

In order to investigate the cleaved surfaces in more detail, we investigate the core level spectra obtained using x-ray photoemission spectroscopy employing Al $K\alpha$ source (XPS) and significantly bulk sensitive case with hard x-ray photoemission (HXP). The Se $3d$ spectra, shown in Fig. 5(a), exhibit difference in the lineshape of the spectra from S1 and S2 surfaces. Signature of three distinct features could be observed in the spectra as marked by '1', '2' and '3' at the binding energies 53.55 eV, 53.25 eV and 53.05 eV, respectively. A change in emission angle from normal emission to 60° off-normal emission from the S1 surface containing Se1 as the surface termination exhibit additional modification of the lineshape. At 60° emission, the electron escape depth, λ becomes half of its normal emission value of about 20Å [25, 26]. On the other hand, the Se $3d$ spectrum from hard x-ray photoemission corresponding to a λ value close to 40Å will represent essentially the bulk electronic structure [27, 28]. The HXP spectrum from S1 surface peaks at 53.25 eV and 54.1 eV binding energies representing spin-orbit split Se $3d_{5/2}$ (Peak '2') and $3d_{3/2}$ features, respectively. The presence of the component peaks are verified by fitting the data at different surface sensitivities consistently [29]. A typical case is shown in Fig. 5(a). The feature '1' becomes relatively stronger in the XPS spectrum and enhances further with the increase in surface sensitivity. Thus, the features '1' and '2' can be attributed to the surface and bulk Se in the case of Se1 terminated surface. The feature '3' has been attributed to the photoemission core level signal from Se2 in the Bi terminated case (S2). Since, Se2 is sandwiched by two Bi layers from both sides with strong hybridization, the Se $3d$ core hole will be better screened in this case compared to the core hole in Se1 layers in other cases. This will lead to a relatively lower binding energy for the corresponding core level feature. These results clearly demonstrate the identification of S1 and S2 termination in these measurements.

We observe that the freshly cleaved sample do not show signature of any impurity feature in the XPS spectrum. With the aging of the cleaved surface, oxygen signal appears and gradually grows up with time delay [6]. Typical spectra at 6 hrs delay is shown in Fig. 5(b). There are three distinct features, A, B and C in the O $1s$ signal. The feature B is not observed in the O $1s$ signal from S2 surface indicating its relation to the bonding to surface Se-layers in S1 case.

All the above results suggest that the energy shift of the Dirac point occurs due to the adsorption of oxygen on the sample surface. Such energy shift has also been predicted in the band structure results shown in Fig. 2(e). Interestingly the trend observed in the calculation matches well with the experimental results indicating such energy shift to be a simple band structure effect. Se and O belong to the same group in the Periodic table with O being the topmost element with higher electronegativity. Therefore, O on Se surface forms SeO_x complex. Se-O bonding will attract electron cloud from the neighborhood reducing the electron density in the other Bi-Se neighborhoods. Since the conduction band consists of Bi $6p$ and Se $4p$ electrons, this would lead to an effective electron doping in the conduction band. On the other hand, oxygen on Bi-terminated surface would form BiO_x complexes leading to more charge localization in the vicinity of oxygens reducing the Fermi surface volume; an effective hole doping scenario.

It is important to note here that while the Dirac states shifts differently in energy due to aging, the intensity of

the Dirac states gradually decreases with aging as shown in Fig. 4(g) and 4(h) for both the surface terminations. This demonstrates that the hybridization with the highly electronegative oxygen on the sample surface leads to a partial breakdown of the connectivity of the surface states to the bulk that presumably induces fragility in the topological order leading to the emergence of simple two-dimensional surface states. While there have been several observation of the surface band bending induced by adsorption of residual gases [17, 30–32], more studies are required to investigate such competing behavior of the topological order and the simple surface state behavior.

CONCLUSIONS

In summary, we studied the detailed electronic structure of a typical topological insulator, Bi_2Se_3 employing high resolution photoemission spectroscopy and ab initio band structure calculations. In our study, the same sample could be cleaved to different surface terminations that enabled us to study the role of surface termination on the topological order without any influence from the change in impurity/defect level in this system. The Dirac cone representing the topological order of the surface states shifts in energy with aging due to the accumulation of oxygen impurities on the sample surface. The energy shift is different on Se and Bi terminated surfaces. In addition, the surface impurities seem to induce fragility in the topological order of the surface states.

ACKNOWLEDGEMENTS

This article is dedicated to Prof. D. D. Sarma for his insightful teaching, inspirations and affections all along. The financial support from DAE, Govt. of India & the DST-DESY project to perform the experiments at P09 beamline at PETRA III, Hamburg, Germany are thankfully acknowledged. We acknowledge Dr. Indranil Sarkar for his help during the measurements at PETRA III beamline. The samples were prepared by Prof. G. Balakrishnan with the financial support from EPSRC, UK (EP/L014963/1).

* Corresponding author: kbmaiti@tifr.res.in

[1] M. Z. Hasan, C. L. Kane. Topological insulators. Rev. Mod. Phys. **82**, 3045 (2010).

[2] L. Fu, C. L. Kane, E. J. Mele. Topological Insulators in Three Dimensions. Phys. Rev. Lett. **98**, 106803 (2007).

[3] C. L. Kane, E. J. Mele. Superconducting Proximity Effect and Majorana Fermions at the Surface of a Topological Insulator. Phys. Rev. Lett. **95**, 226801 (2005).

[4] B. A. Bernevig, T. L. Hughes, S. C. Zhang. Quantum Spin Hall Effect and Topological Phase Transition in HgTe Quantum Wells. Science **314**, 1757 (2006).

[5] D. Hsieh, Y. Xia, D. Qian, L. Wray, J. H. Dil, F. Meier, J. Osterwalder, L. Patthey, J. G. Checkelsky, N. P. Ong, A. V. Fedorov, H. Lin, A. Bansil, D. Grauer, Y. S. Hor, R. J. Cava, M. Z. Hasan. A tunable topological insulator in the spin helical Dirac transport regime. Nature **460**, 1101 (2009)

[6] D. Biswas, S. Thakur, K. Ali, G. Balakrishnan, and K. Maiti. Anomalies of a topologically ordered surface. Sci. Rep. **5**, 10260 (2015); *ibid.* Aging of the surface of Bi_2Se_3. arXiv: 1411.0801v1.

[7] D. Biswas and K. Maiti. Surface-interface anomalies and topological order in Bi_2Se_3. EPL **110**, 17001 (2015); *ibid.* Anomalies in the electronic structure of Bi_2Se_3. arXiv: 1502.03631v1.

[8] D. D. Reis *et al.* Surface structure of Bi_2Se_3(111) determined by low-energy electron diffraction and surface x-ray diffraction. Phys. Rev. B **88**, 041404(R) (2013).

[9] L. V . Yashina, J. S.-Barriga, M. R. Scholz, A. A. Volykhov, A. P . Sirotina, V. S. Neudachina, M. E. Tamm, A. Varykhalov, D. Marchenko, G. Springholz, G. Bauer, A. K.-Gericke, O. Rader. Negligible Surface Reactivity of Topological Insulators Bi_2Se_3 and Bi_2Te_3 towards Oxygen and Water. ACS Nano **7**, 5181 (2013).

[10] V. V. Atuchin, V. A. Golyashov, K. A. Kokh, I. V. Korolkov, A. S. Kozhukhov, V. N. Kruchinin, S. V. Makarenko, L. D. Pokrovsky, I. P. Prosvirin, K. N. Romanyuk, O. E. Tereshchenko. Formation of Inert Bi_2Se_3(0001) Cleaved Surface. Cryst. Growth Des. **11**, 5507 (2011).

[11] V. A. Golyashov, K. A. Kokh, S. V. Makarenko, K. N. Romanyuk, I. P. Prosvirin, A. V. Kalinkin, O. E. Tereshchenko, A. S. Kozhukhov, D. V. Sheglov, S. V. Eremeev, S. D. Borisova, E. V. Chulkov. Inertness and degradation of (0001) surface of Bi_2Se_3 topological insulator. J. Appl. Phys. **112**, 113702 (2012).

[12] D. Kong, J. J. Cha, K. Lai, H. Peng, J. G. Analytis, S. Meister, Y. Chen, H.-J. Zhang, I. R. Fisher, Z.-X. Shen, Y. Cui. Rapid Surface Oxidation as a Source of Surface Degradation Factor for Bi_2Se_3. ACS Nano **5**, 4698 (2011).

[13] H.-J. Noh, H. Koh, S.-J. Oh, J.-H. Park, H.-D. Kim, J. D. Rameau, T. V alla, T. E. Kidd, P. D. Johnson, Y. Hu, Q. Li. Spin-orbit interaction effect in the electronic structure of Bi_2Te_3 observed by angle-resolved photoemission spectroscopy. EPL **81**, 57006 (2008).

[14] H. Lin, T. Das, Y. Okada, M. C. Boyer, W. D. Wise, M. Tomasik, B. Zhen, E. W. Hudson, W. Zhou, V. Madhavan, C.-Y. Ren, H. Ikuta and A. Bansil. Topological Dangling Bonds with Large Spin Splitting and Enhanced Spin Polarization on the Surfaces of Bi_2Se_3. Nano Lett. **13**, 1915 (2013).

[15] Benia, H. M., Lin, C., Kern, K. & Ast, C. R. Reactive Chemical Doping of the Bi_2Se_3 Topological Insulator. Phys. Rev. Lett. **107**, 177602 (2011).

[16] P. D. C. King *et al.* Large Tunable Rashba Spin Splitting of a Two-Dimensional Electron Gas in Bi_2Se_3. Phys. Rev. Lett. **107**, 096802 (2011).

[17] M. Bianchi, D. Guan, S. Bao, J. Mi, B. B. Iversen, P. D. C. King and P. Hoffman. Coexistence of the topological state and a two-dimensional electron gas on the surface of Bi_2Se_3. Nat. Commun. **1**, 128 (2010).

[18] P. Blaha, K. Schwarz, G.K.H. Madsen, D. Kvasnicka and J. Luitz, WIEN2k An Augmented Plane Wave + Local Orbitals Program for Calculating Crystal Properties, K. Schwarz, Techn. Universitt Wien, Austria, 2001. ISBN 3-9501031-1-2.

[19] M. I. Zargarova, P.K. Babaeva, D.S. Azhdarova, Z.D. Melikova, S.A. Mekhtieva. Bi-Cu-In-Se Links to Phase Diagram Literature. Inorg. Mater. **31**, 263-264 (1995).

[20] J. P. Perdew, K. Burke, M. Emzerhof. Generalized Gradient Approximation Made Simple. Phys. Rev. Lett. **77**, 3865 (1996).

[21] K. Maiti, V. R. R. Medicherla, S. Patil, R. S. Singh. Revelation of the Role of Impurities and Conduction Electron Density in the High Resolution Photoemission Study of Ferromagnetic Hexaborides. Phys. Rev. Lett. **99**, 266401 (2007).

[22] K. Maiti. Role of vacancies and impurities in the ferromagnetism of semiconducting CaB_6. EPL **82**, 67006 (2008).

[23] K. Maiti, R. S. Singh, V. R. R. Medicherla, Observation of particle hole asymmetry and phonon excitations in non-Fermi-liquid systems: A high-resolution photoemission study of ruthenates, EPL **78**, 17002 (2007).

[24] Y. L. Chen, J.-H. Chu, J. G. Analytis, Z. K. Liu, K. Igarashi, H.-H. Kuo, X. L. Qi, S. K. Mo, R. G. Moore, D. H. Lu, M. Hashimoto, T. Sasagawa, S. C. Zhang, I. R. Fisher, Z. Hussain, Z. X. Shen. Massive Dirac Fermion on the Surface of a Magnetically Doped Topological Insulator. Science **329**, 659 (2010).

[25] K. Maiti, U. Manju, S. Ray, P. Mahadevan, I. H. Inoue, C. Carbone, D. D. Sarma. Understanding the bulk electronic structure of $Ca_{1-x}Sr_xVO_3$. Phys. Rev. B **73**, 052508 (2006).

[26] R. S. Singh, V. R. R. Medicherla, K. Maiti, E. V. Sampathkumaran. Evidence for strong 5*d* electron correlations in the pyrochlore $Y_2Ir_2O_7$ studied using high-resolution photoemission spectroscopy. Phys. Rev. B **77**, 201102(R) (2008).

[27] S. Thakur *et al.* Surface bulk differences in a conventional superconductor, ZrB_{12}. J. Appl. Phys. **114**, 053904 (2013).

[28] K. Maiti *et al.* Doping dependence of the chemical potential and surface electronic structure in $YBa_2Cu_3O_{6+x}$ and $La_{2-x}Sr_xCuO_4$ using hard *x*-ray photoemission spectroscopy. Phys. Rev. B **80**, 165132 (2009).

[29] R. S. Singh, K. Maiti, Manifestation of screening effects and A-O covalency in the core level spectra of A site elements in the ABO_3 structure of $Ca_{1-x}Sr_xRuO_3$, Phys. Rev. B **76**, 085102 (2007).

[30] N. Fukui, T. Hirahara, T. Shirasawa, T. Takahashi, K. Kobayashi and s. Hasegawa. Surface relaxation of topological insulators: Influence on the electronic structure. Phys. Rev. B **85**, 115426 (2012).

[31] X. Wang, G. Bian, T. Miller and T.-C. Chiang. Fragility of Surface States and Robustness of Topological Order in Bi_2Se_3 against Oxidation. Phys. Rev. Lett. **108**, 096404 (2012).

[32] Z. Zhang, J. T. Yates Jr. Band Bending in Semiconductors: Chemical and Physical Consequences at Surfaces and Interfaces. Chem. Rev. **112**, 5520 (2012).